

# Computing Quasi-Normal Modes of Schwarzschild Black Holes with Physics-Informed Neural Networks

## Supervisor Progress Presentation

Jonathan Chung

University of Cambridge

25 February 2026

# Outline

# What Are Quasi-Normal Modes?

- A perturbed Schwarzschild black hole emits gravitational radiation as it settles down — the **ringdown**.
- The ringdown consists of **quasi-normal modes** (QNMs): damped sinusoids

$$\Phi(t) \propto e^{-t/\tau} \cos(\omega t)$$

- The frequency  $\omega$  and decay time  $\tau$  depend **only on the black hole mass  $M$**  (for Schwarzschild).
- **Goal:** Solve the perturbation equations numerically to extract  $\omega$  and  $\tau$ .

# From Einstein's Equations to a Master Equation

Start with the Schwarzschild metric and add a small perturbation:

$$g_{\mu\nu} = g_{\mu\nu}^0(\text{Schwarzschild}) + h_{\mu\nu}(\text{small})$$

## Key simplifications:

- ① Linearise Einstein's equations in  $h_{\mu\nu}$ .
- ② Decompose  $h_{\mu\nu}$  in **tensor spherical harmonics** — angular dependence separates.
- ③ Construct a gauge-invariant **master function**  $\Phi$  from the metric perturbation components.

Result: a single 1+1D wave equation for each angular mode  $\ell$ :

$$\boxed{-\frac{\partial^2 \Phi}{\partial t^2} + \frac{\partial^2 \Phi}{\partial x^2} - V(r) \Phi = 0}$$

where  $x = r + 2M \ln\left(\frac{r}{2M} - 1\right)$  is the **tortoise coordinate**.

# The Potentials

The potential  $V(r)$  depends on the **parity** of the perturbation:

**Odd-parity (axial) — Regge–Wheeler:**

$$V_{\text{RW}} = \left(1 - \frac{2M}{r}\right) \left[ \frac{\ell(\ell+1)}{r^2} - \frac{6M}{r^3} \right]$$

**Even-parity (polar) — Zerilli:**

$$V_{\text{Z}} = \left(1 - \frac{2M}{r}\right) \frac{2n^2(n+1)r^3 + 6n^2Mr^2 + 18nM^2r + 18M^3}{r^3(nr+3M)^2}$$

where  $2n = (\ell - 1)(\ell + 2)$ .

- Both potentials peak near  $x \sim 1M$  and vanish at the horizon and infinity.
- A transformation connects them (Chandrasekhar)  $\Rightarrow$  **same QNMs**.
- We focus on the **Zerilli potential** with  $\ell = 2$  (dominant mode).

# Boundary & Initial Conditions

**Boundary conditions** (Sommerfeld — radiation conditions):

$$\text{Horizon } (x \rightarrow -\infty) : (\partial_t - \partial_x) \Phi = 0 \quad (\text{ingoing})$$

$$\text{Infinity } (x \rightarrow +\infty) : (\partial_t + \partial_x) \Phi = 0 \quad (\text{outgoing})$$

**Initial conditions** — outgoing Gaussian pulse:

$$\Phi(x, 0) = \exp \left[ -\frac{(x - 4M)^2}{(5M)^2} \right]$$

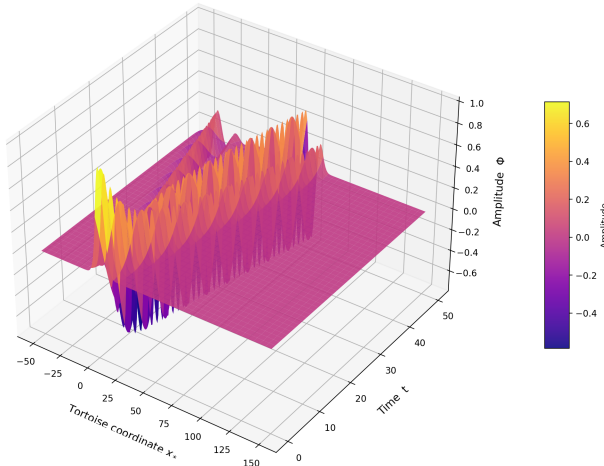
$$\partial_t \Phi(x, 0) = -\partial_x \Phi(x, 0) \quad (\text{purely right-moving})$$

**Domain:**  $x/M \in [-50, 150]$ ,  $t/M \in [0, 50]$ .

The pulse scatters off the potential barrier  $\Rightarrow$  ringdown at late times.

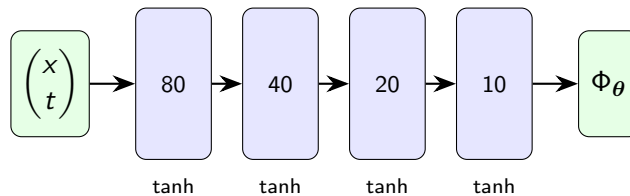
# Ringdown Waveform — 3D Visualisation

3D Waveform of Schwarzschild Black Hole Ringdown (FD Reference)



# Physics-Informed Neural Networks — Core Idea

Instead of a grid, train a neural network  $\Phi_\theta(x, t)$  to satisfy the PDE, BCs, and ICs simultaneously.



- 4 hidden layers, tanh activation, Glorot uniform initialisation.
- Output transform:  $\Phi_\theta = \text{Atanh}(\text{raw output})$  bounds the solution to  $[-1, 1]$ .
- Derivatives via **automatic differentiation** (exact, no discretisation error).
- **4,521 trainable parameters.**

# The Loss Function

Train by minimising a weighted sum of 7 terms:

$$\mathcal{L} = \lambda \cdot [\underbrace{\mathcal{L}_r, \mathcal{L}_{r_x}, \mathcal{L}_{r_t}}_{\text{PDE residual}}, \underbrace{\mathcal{L}_{ic}, \mathcal{L}_{iv}}_{\text{initial condns.}}, \underbrace{\mathcal{L}_{bl}, \mathcal{L}_{br}}_{\text{boundary condns.}}]$$

Term	Penalises	Points	$\lambda$
$\mathcal{L}_r$	$\Phi_{tt} - \Phi_{xx} + V\Phi \neq 0$	$N_r = 32,000$	100
$\mathcal{L}_{r_x}, \mathcal{L}_{r_t}$	Gradients of residual (gPINN)	same	100, 100
$\mathcal{L}_{ic}$	Initial profile mismatch	$N_i = 800$	1
$\mathcal{L}_{iv}$	Initial velocity mismatch	same	100
$\mathcal{L}_{bl}, \mathcal{L}_{br}$	Sommerfeld BC violations	$N_b = 400$	1, 1

- **Phase problem:**  $\Phi(x, t + \alpha)$  is also a solution  $\Rightarrow$  weight  $\lambda_{iv}$  heavily to lock the correct phase.
- Total: **33,600 collocation points** (vs. 500,000 grid points for FD).

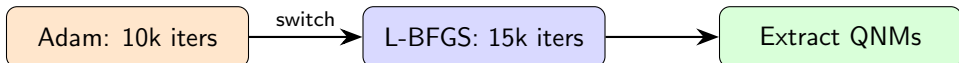
# Two-Phase Training

## Phase 1: Adam (10,000 iters)

- Stochastic gradient descent with adaptive learning rate ( $\text{lr} = 10^{-3}$ ).
- Good at rough, global exploration.
- Uniform point resampling every 100 iters.

## Phase 2: L-BFGS (15,000 iters)

- Quasi-Newton: approximates inverse Hessian from gradient history.
- Fast, precise convergence near minima.
- Sensitive to point changes  $\Rightarrow$  only uniform resampling here.



# Finite Difference Baseline

For comparison, we solve the same PDE with standard numerical methods:

- Uniform mesh:  $N_x = 1,000$  points,  $\Delta x = 0.2M$ .
- Method of lines + 4th-order Runge–Kutta,  $\Delta t = 0.1M$ .
- 500 time steps  $\Rightarrow N_F = 500,000$  grid points.

The FD solution serves as **ground truth** for evaluating the PINN.

## Key comparison:

	FD	PINN
Representation	Grid values $\Phi_{i,j}$	Neural network $\Phi_\theta(x, t)$
Derivatives	FD stencils (approx.)	Autograd (exact)
Points	500,000	33,600
Time-stepping	Explicit RK4	None (global solve)

# Extracting Quasi-Normal Modes

Sample  $\Phi(x_q, t)$  at observation point  $x_q = 10M$ , restrict to late times.

**Method 1 — FFT + Envelope:**

- $\omega$ : FFT of  $\Phi(x_q, t) \Rightarrow$  peak frequency.
- $\tau$ : Linear fit to  $\ln |\text{envelope peaks}|$  vs.  $t \Rightarrow$  slope  $= -1/\tau$ .

**Method 2 — Direct curve fit:**

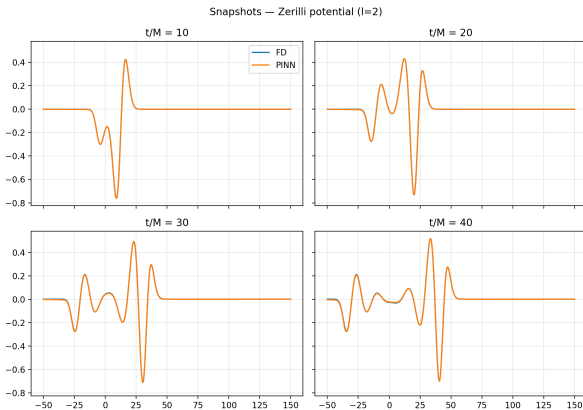
- Fit  $\Phi \approx A e^{-t/\tau} \cos(\omega t + \phi)$  directly via nonlinear least squares.

Compare extracted  $(\omega, \tau)$  against theoretical values (Leaver 1985):

$\ell$	$\omega M$	$\tau/M$
2	0.3737	11.241

# Paper Reproduction: Baseline Results

Reproduced the setup of Patel, Aykutalp & Laguna (2024) with our corrected outgoing initial velocity profile.



Zerilli  $\ell = 2$  QNM Extraction

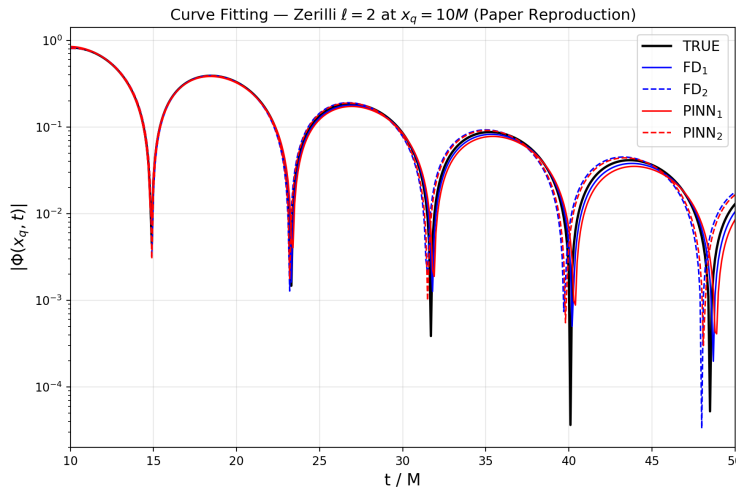
	$\tau/M$	$\omega M$
<b>TRUE</b>	11.241	0.3737
<b>FD<sub>1</sub></b>	10.929 (2.78)	0.3716 (0.56)
<b>FD<sub>2</sub></b>	11.465 (2.00)	0.3798 (1.63)
<b>PINN<sub>1</sub></b>	10.671 (5.07)	0.3697 (1.08)
<b>PINN<sub>2</sub></b>	11.410 (1.50)	0.3784 (1.25)

Parentheses: % error vs. Leaver 1985.

Subscript 1 = FFT + envelope.

Subscript 2 = direct curve fit.

# Curve Fitting — Paper Reproduction



$\log |\Phi|$  vs.  $t/M$  at  $x_q = 10M$ . All five reconstructed damped cosines  $A e^{-t/\tau} \cos(\omega t + \phi)$  overlap closely — both FD and PINN extract QNMs within  $\sim 1\text{--}4\%$  of the Leaver (1985) values.

# QNM Accuracy: Our Results vs. the Paper

Zerilli  $\ell = 2$  —  $\tau/M$  and  $\omega M$  percentage errors

	Paper (Patel et al.)		Ours	
	$\tau/M$ (% err)	$\omega M$ (% err)	$\tau/M$ (% err)	$\omega M$ (% err)
<b>FD</b> <sub>1</sub>	10.804 (3.89)	0.370 (0.90)	10.929 (2.78)	0.372 (0.56)
<b>FD</b> <sub>2</sub>	11.073 (1.49)	0.378 (1.26)	11.465 (2.00)	0.380 (1.63)
<b>PINN</b> <sub>1</sub>	10.089 (10.25)	0.375 (0.29)	10.671 ( <b>5.07</b> )	0.370 (1.08)
<b>PINN</b> <sub>2</sub>	<b>9.620 (14.42)</b>	0.376 (0.52)	<b>11.410 (1.50)</b>	0.378 (1.25)

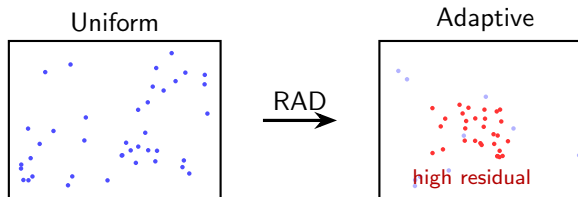
- **Major improvement:** PINN<sub>2</sub> decay time error drops from **14.42%** → **1.50%** (**9.6**× more accurate).
- PINN<sub>1</sub>  $\tau$  error also improves: 10.25% → 5.07% (2.0×).
- Likely cause: our corrected outgoing initial velocity  $\partial_t \Phi = -\partial_x \Phi$  (Sommerfeld condition).

# Our Improvement: Residual-Adaptive Distribution (RAD)

**Problem:** Uniform sampling wastes points in empty regions where  $\Phi \approx 0$ .

**RAD** (Wu et al. 2023): Every  $P$  training steps during Adam—

- ① Generate 100,000 random candidate points.
- ② Evaluate PDE residual  $|r_i|$  at each candidate.
- ③ Compute sampling probability:  $p_i \propto |r_i|^k + c$ .
- ④ Sample 32,000 points from candidates  $\Rightarrow$  replace all domain points.

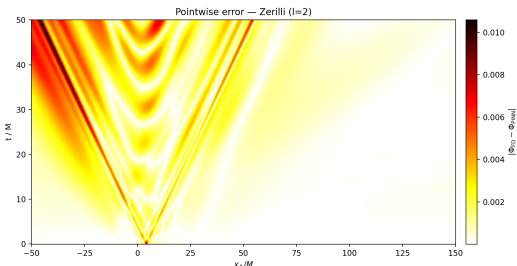


# RAD Tuning Experiments

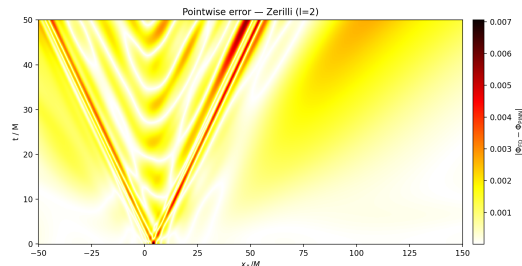
Configuration	$k$	$c$	Final Loss	RMSD	RL2
Uniform (paper repro)	—	—	$1.18 \times 10^{-6}$	0.00183	1.30%
RAD baseline	1	1	$7.40 \times 10^{-7}$	0.00115	0.82%
RAD aggressive	2	0.1	$9.07 \times 10^{-7}$	<b>0.00095</b>	<b>0.67%</b>
RAD $k=2, P=500$	2	0.1	$1.06 \times 10^{-6}$	0.00105	0.75%
RAD + anchor (20%)	1	1	$8.20 \times 10^{-7}$	0.00141	1.00%

- RAD reduces RMSD by **37%** over uniform sampling.
- Aggressive RAD ( $k=2$ ) achieves the **best RMSD** (0.00095).
- Anchor retention has the **second-lowest loss** ( $8.20 \times 10^{-7}$ ) but the **highest RMSD** among RAD runs — suggests over-fitting to anchor points at the expense of global accuracy.

# Spatial Error Distribution



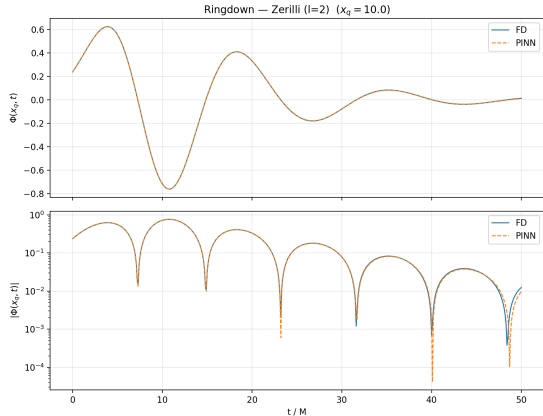
Uniform sampling



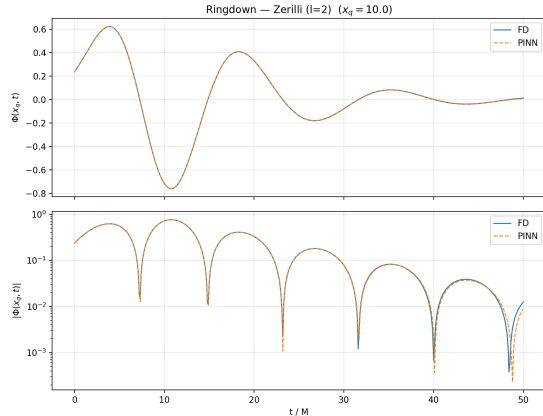
RAD adaptive sampling

RAD reduces the error concentration at the **wavefront leading edge**.

# Ringdown Waveform at $x_q = 10M$



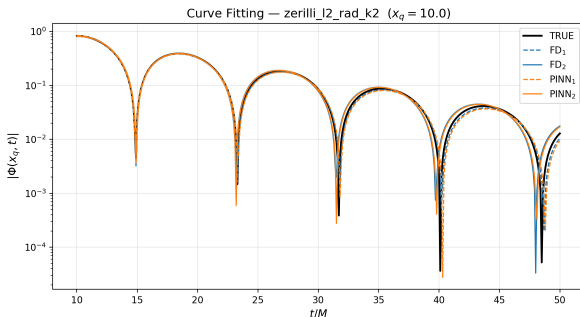
RAD baseline: PINN vs. FD (raw waveforms)



RAD  $k = 2$ : PINN vs. FD (raw waveforms)

Top: linear scale; Bottom:  $\log |\Phi|$ . Both variants closely match the FD reference.

# Curve Fitting — RAD $k=2$



$\log |\Phi|$  vs.  $t/M$  at  $x_q = 10M$  (RAD  $k=2$ )

## Zerilli $\ell = 2$ — QNM Extraction

	$\tau/M$	$\omega M$
<b>TRUE</b>	11.241	0.3737
<b>FD<sub>1</sub></b>	10.929 (2.78)	0.3716 (0.56)
<b>FD<sub>2</sub></b>	11.465 (2.00)	0.3798 (1.63)
<b>PINN<sub>1</sub></b>	10.831 (3.65)	0.3705 (0.85)
<b>PINN<sub>2</sub></b>	11.443 (1.80)	0.3790 (1.43)

FD<sub>1,2</sub> identical to paper repro  
(same FD solver).

PINN<sub>1,2</sub> from RAD  $k=2$  run.

- RAD PINN<sub>2</sub>:  $\tau$  error 1.80% vs. 1.50% (paper repro) — comparable accuracy.
- RAD primarily improves **spatial** accuracy (RMSD), not QNM extraction.

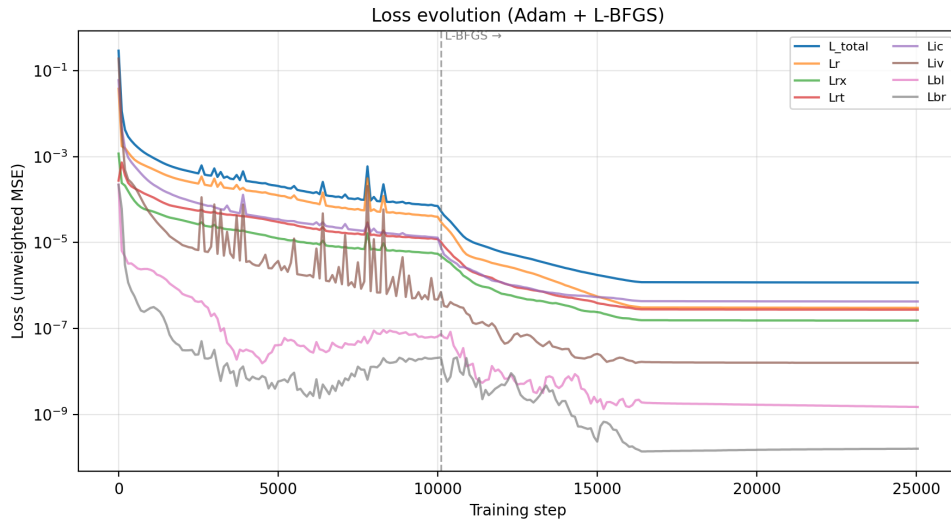
# Summary of Findings

- ① **PINNs can compute QNMs** of Schwarzschild black holes to within  $\sim 1\text{--}2\%$  of known values, using  $15\times$  fewer collocation points than FD.
- ② **RAD adaptive sampling** improves solution accuracy by  $\sim 37\%$  (RMSD) over uniform sampling, by concentrating points where the PDE residual is largest.
- ③ **Aggressive RAD** ( $k = 2$ ) provides the best spatial accuracy (lowest RMSD/RL2). Anchor retention has the second-lowest loss but the highest RMSD among RAD runs — over-fitting to anchor points.
- ④ **Exponential reweighting fails** — naively amplifying late-time residuals destabilises training ( $\tau$  error  $> 20\%$ ).

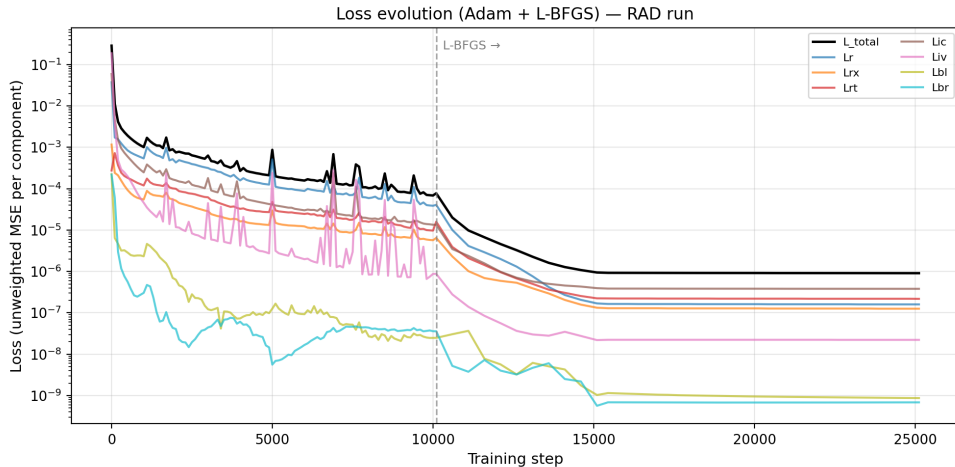
Thank you

Questions?

# Appendix: Loss History — Reproduction Run (Uniform Sampling)



# Appendix: Loss History — RAD Adaptive Sampling



# Appendix: QNM Extraction — Method 1 (FFT + Envelope)

Extract  $\omega$  and  $\tau$  **independently** from the late-time waveform  $\Phi(x_q, t)$ .

## Step 1 — Estimate $\omega$ via FFT:

- ① Window the signal between  $t_{\text{start}}$  and  $t_{\text{end}}$ ; subtract the mean.
- ② Apply a Hann window to reduce spectral leakage.
- ③ Zero-pad by  $64\times$  and compute the real FFT.
- ④ Locate the magnitude peak; refine with **parabolic interpolation** for sub-bin accuracy.
- ⑤ Convert:  $\omega = 2\pi f_{\text{peak}}$ .

## Step 2 — Estimate $\tau$ via log-linear envelope fit:

- ① Find all local maxima of  $|\Phi(x_q, t)|$  (envelope peaks).
- ② Since the envelope decays as  $A e^{-t/\tau}$ , take the logarithm:

$$\ln |y_{\text{peaks}}| = \ln A - \frac{t}{\tau}.$$

- ③ A linear fit gives slope  $m = -1/\tau$ , hence  $\tau = -1/m$ .

# Appendix: QNM Extraction — Method 2 (Nonlinear Curve Fit)

Fit the full damped-cosine model **simultaneously** to the waveform:

$$\Phi(x_q, t) \approx A e^{-t/\tau} \cos(\omega t + \phi).$$

## Procedure:

- ① Obtain initial guesses from Method 1:  $\omega_0, \tau_0$ .
- ② Set  $A_0 = \max |\Phi|$ ,  $\phi_0 = 0$ .
- ③ Run `scipy.optimize.curve_fit` (Levenberg–Marquardt) with four free parameters ( $A, \tau, \omega, \phi$ ).

## Advantages over Method 1:

- All four parameters are fitted **jointly**, so correlations between  $\omega$  and  $\tau$  are captured.
- Uses **every data point**, not just envelope peaks  $\Rightarrow$  typically more accurate.

## Disadvantage:

- Requires good initial guesses; can fail to converge if the signal is noisy or the window is too short.

# Appendix: L-BFGS — Motivation & Core Idea

## Why two optimisers?

- **Adam** (Phase 1): stochastic, handles noisy/flat loss landscapes well; reaches a rough neighbourhood of the minimum quickly.
- **L-BFGS** (Phase 2): quasi-Newton method that uses curvature information to converge much faster once we are near a minimum.

**Full BFGS recap.** Newton's method updates parameters via  $\theta_{k+1} = \theta_k - H_k^{-1} \nabla \mathcal{L}_k$ , where  $H_k$  is the Hessian. Computing and inverting  $H$  is  $O(n^2)$  storage and  $O(n^3)$  per step ( $n$  = number of parameters) — **impractical for neural networks**.

**BFGS** (Broyden–Fletcher–Goldfarb–Shanno) avoids forming the Hessian explicitly. Instead it maintains an *approximate inverse Hessian*  $B_k^{-1}$  and updates it each step using only gradient differences:

$$s_k = \theta_{k+1} - \theta_k, \quad y_k = \nabla \mathcal{L}_{k+1} - \nabla \mathcal{L}_k.$$

## Appendix: L-BFGS — The BFGS Update

The rank-2 update of the *approximate inverse Hessian*  $B_k^{-1}$ :

$$B_{k+1}^{-1} = (I - \rho_k s_k y_k^T) B_k^{-1} (I - \rho_k y_k s_k^T) + \rho_k s_k s_k^T, \quad \rho_k = \frac{1}{y_k^T s_k}.$$

This ensures  $B_{k+1}$  satisfies the **secant condition**  $B_{k+1} s_k = y_k$  while staying symmetric positive-definite.

The search direction is then:

$$d_k = -B_k^{-1} \nabla \mathcal{L}_k$$

followed by a **line search** along  $d_k$  to find the step size.

**Problem:** Still  $O(n^2)$  storage for the dense matrix  $B^{-1}$  — too expensive when  $n$  is the number of neural network weights.

# Appendix: L-BFGS — Limited-Memory Variant

**L-BFGS** (Limited-memory BFGS) solves the storage problem:

- Store only the last  $m$  pairs  $\{s_k, y_k\}$  (typically  $m = 20\text{--}50$ ).
- Reconstruct the matrix–vector product  $B_k^{-1}\nabla\mathcal{L}$  on-the-fly via a **two-loop recursion** — never form  $B^{-1}$ .
- Storage:  $O(mn)$  instead of  $O(n^2)$ ; each step is  $O(mn)$ .

**Two-loop recursion** (Nocedal 1980):

- ➊ *Backward pass*: for  $i = k-1, \dots, k-m$ , compute scalar  $\alpha_i = \rho_i s_i^T q$  and set  $q \leftarrow q - \alpha_i y_i$ .
- ➋ *Scale*:  $r \leftarrow H_k^0 q$  (diagonal initialisation).
- ➌ *Forward pass*: for  $i = k-m, \dots, k-1$ , set  $r \leftarrow r + s_i(\alpha_i - \rho_i y_i^T r)$ .
- ➍ *Search direction*:  $d_k = -r$ .

**In our pipeline:**

- Adam runs for 10 k steps  $\Rightarrow$  L-BFGS refines for 15 k steps.
- L-BFGS uses *full-batch* gradients (all 33 600 points), giving accurate curvature estimates.
- Typically reduces the loss by a further 1–2 orders of magnitude.

## Appendix: Finite Difference Solver — Method of Lines

Rewrite the PDE  $\Phi_{tt} - \Phi_{xx} + V\Phi = 0$  as a **first-order system**:

$$u = \Phi, \quad v = \Phi_t, \quad \begin{cases} u_t = v, \\ v_t = u_{xx} - V(x) u. \end{cases}$$

**Spatial discretisation** (2nd-order central differences):

$$u_{xx}|_i \approx \frac{u_{i+1} - 2u_i + u_{i-1}}{\Delta x^2}, \quad 1 \leq i \leq N_x - 2.$$

At boundaries ( $i = 0$  and  $i = N_x - 1$ ): 2nd-order **one-sided** stencils, e.g.

$$u_{xx}|_0 \approx \frac{2u_0 - 5u_1 + 4u_2 - u_3}{\Delta x^2}.$$

This converts the PDE into a system of ODEs in time:  $\dot{\mathbf{U}}(t) = \mathbf{F}(\mathbf{U}(t))$ , where  $\mathbf{U} = (u_0, \dots, u_{N_x-1}, v_0, \dots, v_{N_x-1})$ .

# Appendix: Finite Difference Solver — RK4 & Boundary Conditions

## Time integration — Classical RK4:

$$\mathbf{U}^{n+1} = \mathbf{U}^n + \frac{\Delta t}{6} (\mathbf{k}_1 + 2\mathbf{k}_2 + 2\mathbf{k}_3 + \mathbf{k}_4),$$

where  $\mathbf{k}_1 = \mathbf{F}(\mathbf{U}^n)$ ,  $\mathbf{k}_2 = \mathbf{F}(\mathbf{U}^n + \frac{\Delta t}{2}\mathbf{k}_1)$ , etc.

4th-order accuracy in time; requires  $\Delta t / \Delta x \leq 1$  (CFL condition). We use  $\Delta x = 0.2M$ ,  $\Delta t = 0.1M$   
⇒ CFL ratio = 0.5.

## Sommerfeld radiative BCs (applied at every RK4 sub-step):

$$\text{Left } (x \rightarrow -\infty) : (\partial_t - \partial_x)\Phi = 0 \Rightarrow v_0 = u_x|_0,$$

$$\text{Right } (x \rightarrow +\infty) : (\partial_t + \partial_x)\Phi = 0 \Rightarrow v_{N_x-1} = -u_x|_{N_x-1}.$$

Spatial derivatives  $u_x$  at boundaries use 2nd-order one-sided stencils:

$$u_x|_0 \approx \frac{-3u_0 + 4u_1 - u_2}{2\Delta x}, \quad u_x|_{N_x-1} \approx \frac{3u_{N_x-1} - 4u_{N_x-2} + u_{N_x-3}}{2\Delta x}.$$